Post-print of: Darowicki K., Janicka E., Mielniczek M., Zieliński A., Gaweł Ł., Mitzel J., Hunger J.: The influence of dynamic load changes on temporary impedance in hydrogen fuel cells, selection and validation of the electrical equivalent circuit. APPLIED ENERGY. Vol. 251 (2019). DOI: 10.1016/j.apenergy.2019.113396

The Influence of dynamic load changes on temporary impedance in hydrogen fuel cells, selection and validation of the electrical equivalent circuit

K. Darowicki[(1)], E. Janicka[(1)*], M. Mielniczek[(1)], A. Zielinski[(1)],L. Gawel[(1)], J. Mitzel[(2)], J. Hunger[(3)]

[(1)] Department of Electrochemistry, Corrosion and Materials Engineering
Chemical Faculty, Gdansk University of Technology
11/12 Narutowicza, 80-233 Gdansk, POLAND

[(2)] Institute of Engineering, Thermodynamics, Electrochemical Energy Technology
Pfaffenwaldring 38-40, 70569 Stuttgart, GERMANY

[(3)] Zentrum für Sonnenenergie- und Wasserstoff-Forschung Baden-Württemberg (ZSW)
Helmholtzstraße 8, 89081 Ulm, GERMANY

Abstract

To achieve optimal performance of a fuel cell, a reliable monitoring and diagnostic method is required. The currently utilized methods give limited information or they are impossible to use under dynamic working conditions. To obtain comprehensive information about the fuel cell operation we utilized novel dynamic electrochemical impedance spectroscopy. Impedance measurements in dynamic mode were performed on a hydrogen fuel cell, working under various conditions. By utilizing this new methodology, optimum parameters for cell operation were determined. An electrical equivalent circuit for cathodic processes was determined. Presence of an interlayer, between the membrane and the catalytic layer, was postulated. The instantaneous impedance spectra were analysed under the function of current load. The complete character of the impedance spectra was revealed, and the electrical equivalent circuit was validated. The presence of the interlayer was established by impedance analysis and by a profile of platinum content changes in the membrane electrode assembly. The proposed investigation methodology provides monitoring and diagnostics of fuel cell components, which gives the possibility of streamlined management of the fuel cell operation.

Keywords:

Impedance monitoring; Fuel cell diagnostics; Fuel cell; PEMFC; Equivalent circuit

1. Introduction

A rapid increase in electrical energy demand and a simultaneous emphasis on the reduction of negative environmental impact of these electrical sources means there is a demand for alternative, low-emission energy supplies [1]. A proportion of these electrical needs can be fulfilled by fuel cells [2], with proton-exchange membrane (PEM) fuel cells being the most promising candidate. The characteristic features of PEM cells are the high efficiency of electric energy production and relatively

low heat generation. Their undisputable advantages are their short reaction time in the systems which are subjected to varying load and they have a short start-up time [3]. These features result from the low temperature of the hydrogenation reaction occurring across the membrane, which is typically from 60 to 100 °C. Thanks to these unique properties, fuel cells have been successfully used in micro combined heat and power systems [4] and fuel-cell hybrid vehicles [5].

The main structural element of the hydrogen fuel cell is a membrane–electrode assembly (MEA). This forms the central part is a proton-exchange membrane, most frequently made of Nafion. Catalytic layers (CL) adhere to both sides of the membrane, which are in contact with the gas-diffusion layers (GDL). However, the presence of sharp boundaries between these layers is purely conventional.

The catalytic layer is a region where the electrochemical reactions proceed. This consists of a network of platinum catalyst nanoparticles, deposited on a carbon support and connected with ionomer. Such a structure ensures a developed active surface of platinum, and also allows for fast transport of the reaction gases, products and the continuous flow of electrons. The amount of ionomer on the cathodic-side of the catalytic layer has significant influence on the kinetics of the oxygen reduction reaction via minimization of the impact of H^+ ion transport to the catalyst [6]. The authors of this paper postulate the presence of an interlayer, between the membrane and the catalytic layer, which exhibits the features of both layers.

The role of the GDL is for the uniform distribution of the reagents into the reaction regions and for efficient water drainage [7]. The GDL is a porous material, which plays a key role in the process of the initiation of hydrogen oxidation and oxygen reduction reactions within the catalyst layers. The GDL also improves water management in MEA and it facilitates the permeation of liquid water produced at the cathodic side, which prevents the catalyst layer from flooding and blocking [8]. Niu et al. proposed the most optimal amount PTFE in GDL considering its wettability [9]. The GDL works as a supporting structure and it consists of an electric conductor between the CL and reagent feed region [10], [11].

The consumption of energy changes the physico-chemical characteristics of the fuel cell and its components. Each component can be represented using their electrical quantities such as resistances and capacitances. Thus, the flow of charge is going to change the electrical characteristics of the cell's individual components. The determination of these changes is of fundamental importance from a practical standpoint. Dynamic Electrochemical Impedance Spectroscopy (DEIS) measures the impedance changes of the fuel cell during its operation [12], [13]. Accordingly, there is a possibility to monitor the changes of individual components characteristics in operando [14], [15]. The utilization of this technique to study PEM systems in operando is novel and has not yet been described in the

literature. The determination of the impedance variation *vs* the change in the current enables the optimization of the operation conditions.

The aforementioned issues are addressed in this paper. It should be emphasized that the topic is original because changes of impedance of the PEM hydrogen cell's components in dynamic conditions have not been presented so far. The proposed novel use of DEIS methodology introduces a whole series of advantages for PEMFC impedance measurements when compared to classic EIS methodology. A detailed comparison of results obtained by both EIS and DEIS has been previously discussed by Wysocka *et al.* [16] and Darowicki *et al.* [17]. One of the biggest differences between these two methods is type of perturbation signal. In EIS, the perturbation signals of changing frequency are applied sequentially to investigated object. In the DEIS method, the signal is composed of multiple sine waves with numerous frequencies, which is equivalent to the simultaneous perturbation of the object at all given frequencies. Due to this modification time of obtaining one impedance spectrum, the DEIS method is solely limited to the period of the lowest frequency signal. In EIS the time consists of the sum of periods of all the sampled frequencies. Over the frequency range utilized in this paper, the DEIS allows one to obtain a spectrum in 1 second and it gives the opportunity to study PEMFC under dynamic conditions or its implementation as a characterisation method in operando PEMFC. DEIS can be performed simultaneously with a change in current, this provides us with an advantage over classic methods. With current available techniques it is extremely difficult to comprehensively characterize the processes occurring in the fuel cell under dynamic operation conditions including load changes. Additionally, due to coherency of AC and DC measurements there is a possibility to determine the completeness of the impedance spectra analysis. Moreover, all the obtained results from the impedance analysis can be presented against a current function. Analysing the chi-square results against the current function is a novel approach for determining the quality of the equivalent circuit fitting. Both, controlling and monitoring of the PEMFC operation can be highly improved thanks to implementation of the DEIS method. This is crucial for improving the operation and extending the lifetime of currently available fuel cells. Moreover, it can be a very useful tool in the process of designing new fuel cells.

2. Materials and methods

The fuel cell under investigation was designed and assembled by the Zentrum für Sonnenenergie- und Wasserstoff-Forschung Baden-Württemberg – ZSW (Ulm, Germany). It contained commercially available low loaded MEA with a 96cm^2 active surface.

The flow channels were located on a monopolar plate, in a cascaded flow field design configuration with parallel-connected multiple serpentine groups. The reagents were hydrogen with 99.999 %

purity, and compressed air from an oil-free compressor. The investigations were carried out under the following conditions:

- stack temperature – 80 °C,
- air and hydrogen backpressure - 150 kPa (abs),
- relative humidity of air and hydrogen – 50 %,
- stoichiometry of reagents – in high excess.

The tests were performed using a measurement station consisting of:

- a test bench from the Fuel Cell Technologies Inc. (Albuquerque, USA) containing an electronic load from the Keysight Co. (Santa Rosa, USA),
- a module from National Instruments (Austin, USA) with two measurement cards, PXIe 6164 and PXIe 4497, for generation of a **multi-sinusoidal** AC signal and data acquisition.

The investigations were completed under galvanodynamic mode. The cell load was changed with a rate of 50 mAs^{-1}, over a range from 9 to 115 A. Impedance measurements were performed simultaneously with the change in load. A multi-sinusoidal perturbation signal consisting of 13 elementary sinusoids with frequencies from 5 Hz to 1123 Hz. The amplitudes of sinusoidal components were selected to preserve a linearity condition. For the applied change in load rate and for the frequency range of the AC perturbation, a single impedance spectrum was recorded over a period of one second. A detailed description of the measurement technique has been presented earlier in numerous publications [18,19].

The images of a MEA cross-section were recorded using a Hitachi S3400N scanning electron microscope (SEM) with a tungsten source. A profile of platinum content in MEA was obtained by energy-dispersive X-ray spectroscopy (EDX), using an UltraDry Detector from Thermo Fisher Scientific.

3. Results and discussion

During operation of the fuel cell, an increase in the current consumption is accompanied by a decrease in voltage between the plates, this is a typical current - voltage characteristic of PEMFCs. The dynamics of the processes occurring inside the cell changes, depending on current load. This fact is confirmed by the impedance diagram presented in Fig. 1a.

Fig. 1a.

The impedance diagram is a collection of the individual impedance spectra obtained under dynamic mode during the load change. Simple analysis reveals a range of current magnitude, for which the

measured impedance is at its lowest. It should be associated with the optimum range of the current load. The recorded impedance spectra have a complicated structure, with at least two observable time constants. The isofrequency lines in the high-frequency range do not depend on current and are attributed to structural parameters. The isofrequency lines in a medium- and low-frequency range relate to the amount of generated energy, which pertains to the electrochemical phenomena. The impedance diagram can be converted into a projection showing the changes of complex capacitance versus direct current, as illustrated in Fig. 1b.

Fig. 1b.

The instantaneous complex capacitance spectra reveal the existence of two capacitances. In the low limit range of frequencies, the complex capacitance spectra tend to infinity. The direct current load has a strong influence on the shape of complex capacitance spectra. The spectra take relatively high values for the optimum range of direct current.

Deeper impedance analysis requires the selection of a suitable electrical equivalent circuit. This problem is discussed in the following sections.

3.1. Electrical equivalent circuit

For each instantaneous value of the direct current, the total cell impedance is determined by:

$$Z_{FC}(j\omega, i) = Z_A(j\omega, i) + Z_M(j\omega, i) + Z_C(j\omega, i) \quad (1)$$

where: $Z_{FC}(j\omega, i)$ is the instantaneous impedance of the entire cell, $Z_A(j\omega, i)$ is the instantaneous impedance of the anode, $Z_C(j\omega, i)$ is the instantaneous impedance of the cathode, $Z_M(j\omega, i)$ is the instantaneous impedance of the membrane, i is the instantaneous magnitude of direct current, ω – angular frequency and $j^2 = -1$ – imaginary unit.

Cahan *et al.* [20], with the use of EIS technique, proved that Nafion impedance in the frequency range up to 100 kHz is characterized only by a pure resistor. To fully study impedance of membrane measurements should be carried out for much higher frequencies [21]. Over the applied measurement frequencies range, the impedance of the membrane is represented by resistance given as:

$$Z_M(j\omega, i) \cong R_M(i) \quad (2)$$

where: $R_M(i)$ is the instantaneous resistance of the membrane.

Makharia *et al.* [22] and Reshetenko *et al.* [23] adopted the same assumption in classic impedance measurements.

An exchange current density is three orders of magnitude lower for the oxygen reduction reaction than for the corresponding hydrogen oxidation reaction [24]. Oxygen reduction is a slow reaction when compared to hydrogen oxidation. These relationships were confirmed by studies using a rotating disk electrode made by Singh *et al.* [25] and Paulus *et al.* [26]. Thus, the impedance of the anode is negligible when compared to the impedance of the cathode [27]:

$$Z_A(j\omega, i) \ll Z_C(j\omega, i) \quad (3)$$

It should be noted that this is a simplified assumption as the impedance of the anodic process, which is negligibly low, is present in the $R_M(i)$ value.

To select a proper equivalent circuit, an SEM image of the MEA cross-section was collected (Fig. 2a). From the image, one can distinguish the membrane and the catalyst layers. Moreover, an analysis of the platinum content along the entire thickness of the MEA was conducted, based on the number of counts (Fig. 2b). It was revealed that the Pt content does not change rapidly between the membrane and the catalyst layer regions. Accordingly, the presence of the membrane-catalyst interlayers (MCIs) at the cathodic and anodic sides was postulated. In the MCIs, the Pt content increases with decreasing distance to the catalyst layer. Based on this concept, a scheme of the MEA cathodic part cross-section is proposed (Fig. 2c). This equivalent circuit was previously compared with other commonly used circuits using statistical terms [28].

Fig.2a.

Fig.2b.

The accepted assumptions and presented structure of the MEA leads to the electrical equivalent circuit, considering the main processes occurring at the cathode (Fig. 2c).

Fig. 2c & d

The measurements had an instantaneous character, they were carried out under the dynamic conditions of a load change. To emphasize this observation, an evolution in the magnitude of elements in the equivalent circuit was expressed against the current. The values of $R_{MCI}(i)$ and $C_{MCI}(i)$ are related to the morphology of the interlayer, between the membrane and the catalyst layer. The capacitance of the electrical double layer on the cathode catalyst is described by $C_{DL}(i)$. The charge transfer resistance of the oxygen reduction reaction is represented by $R_{CT}(i)$. Transport of mass to the reaction region is associated with the element $Z_D(j\omega, i)$, which describes the diffusion over a finite thickness layer. Depending on the magnitude of obtained current, the value of mass transport resistance can be determined by different processes. In a low current regime, the

resistance of oxygen transport to the catalyst layer can be regarded as constant and negligibly low; the voltage loss is attributed to the transport of protons from the ionomer to platinum [29]. The authors assume that the transport of air to the catalyst was negligibly small in activation area. However, in the high current density regime, when there is a shortage of reagents or when water blocks the pores in the diffusion layer, it can have a noticeable effect on oxygen transport to the catalyst layer [8].

3.2 Analysis of impedance spectra

The dependences between the instantaneous values of the electrical elements of the equivalent circuit and the current density are presented in Figs 3a-f.

Fig.3a.

Fig. 3a illustrates the evolution of the instantaneous values, $R_{MCI}(i)$ and $R_M(i)$, versus the generated electric energy. The interlayer between the membrane and the catalyst layer contains a significant amount of ionomer and that is why both parameters exhibit the same variations in change. In the low current regime, there is linear decrease in both resistances, which is most probably connected with the amount of water generated in the cell. The values of $R_M(i)$ are twice as high as the $R_{MCI}(i)$ over the entire current range investigated. That is why, the authors suggest that these two quantities are connected and interrelated, so their influence on the total resistance of the cell should not be discussed separately.

Fig.3b.

Fig. 3b presents the changes of the instantaneous values of $C_{DL}(i)$ and $C_{MCI}(i)$ versus the generated electric energy. The interlayer contains platinum nanoparticles; however their content is significantly reduced when compared to the catalyst layer. Hence, both characteristics shown in Fig. 3b have practically the same shape and the $C_{MCI}(i)$ value constitutes ca. 30 % of the $C_{DL}(i)$ value. On the active surface of the catalyst layer, at the cathodic side, the oxygen electro-reduction reaction occurs, which is described by charge transfer resistance and differential double layer capacitance. The oxygen reduction reaction takes place in the low current density range, on the catalyst's surface, which is partially covered with an oxide layer [24]. At low current load of the cell, when the cathode operates at a high potential, platinum oxide is formed, this then disappears with a decrease in cell voltage [30]. These dependences are marked with the dashed lines given as 1' and 1". The differential capacitance of the metallic electrode without an oxide surface is much higher than the capacitance of the surficial oxidized electrode. In the high current density range, the oxygen reduction reaction takes place at the catalyst's surface, which is pure Pt surface [22]. The changes in

the instantaneous capacitances $C_{MCI}(i)$ and $C_{DL}(i)$ on pure platinum are marked with the dashed lines labelled 2' and 2". Their values increase with an increase in the generated energy.

Fig.3c.

The changes of the instantaneous values of $R_{CT}(i)$ against the current are depicted in Fig. 3c. Charge transfer resistance decreases rapidly with an increase in load until a time constant when operation with ohmic losses occur. The minimum for the charge transfer resistance is clearly visible in this region and this indicates the optimum current load range.

Fig. 3d shows the changes of instantaneous values of the diffusion resistance, determined based on instantaneous changes in the impedance of the $Z_D(j\omega, i)$ element, which describes diffusion through a finite thickness layer. The diffusion resistance was calculated using the formulae given as (4) – (5).

$$Z_D(j\omega, i) = \frac{B(i)}{Y_0(i)B(i)\sqrt{j\omega}coth\left(B(i)\sqrt{j\omega}\right)} \quad (4)$$

$$lim_{x\to 0}\frac{B(i)}{Y_0(i)}\frac{1}{xcoth(x)} = \frac{B(i)}{Y_0(i)} = R_D(i) \quad (5)$$

Fig.3d.

Execution of measurements over the entire current range provides an opportunity to determine instantaneous impedance values of the element connected with hydrogen cations or oxygen molecules diffusion to the catalyst. The dependence between $R_D(i)$ and current is similar to the characteristics shown by $R_{CT}(i)$. For the low current values, the diffusion resistance is associated with the transport of protons from the membrane to the catalyst's surface. Its value decreases as the amount of generated energy increases. There is the local minimum, which corresponds to the undisturbed transport of reactants to the catalyst's surface. Together with an increasing the amount of water generated in the cell, the value of the diffusion resistance begins to increase, this is attributed to the more difficult transport of oxygen to the catalytic layer. Moreover, according to the equation 4, the instantaneous impedance $Z_D(j\omega, i)$ can be used to determine changes in the structural coefficient $B(i)$, which describes the thickness of a diffusion layer. Fig. 3e illustrates the changes of the instantaneous values of the $B(i)$ parameter versus the current.

Fig.3e.

The value of the diffusion layer thickness is directly proportional to the changes in the $B(i)$ parameter. Understanding the values of parameter *B* and diffusion coefficient from equation (6), the diffusion layer thickness can be calculated. This is a novel approach to describe the changes of the

diffusion layer thickness during varying conditions of the fuel cell operation. After this short discussion, the changes of $R_D(i)$ versus current load, presented in Fig. 3d, are easier to understand. Increasing diffusion resistance with an increase of current is closely related to the diffusion layer thickness.

$$\delta = B * \sqrt{D} \quad (6)$$

Considering the membrane resistance together with the membrane-catalyst interlayer resistance, it is noted that a sum of these parameters determines the cell resistance in the region of optimum current load (Fig. 3f). The regime of low and very high currents, $R_D(i)$ and $R_{CT}(i)$, have the biggest influence on the value of the resistance. Both parameters exhibit similar characteristics versus the cell load, their minima occur for practically identical values of the current load of the cell.

Fig. 3f.

3.3. Quality of fitting of electrical equivalent circuit to experimental results

In the classic EIS method, $\chi^{2.}$ is a coefficient describing the quality of fitting of the equivalent circuit to the experimental data [31]. χ^2 is a numerical measure of the reliability of the proposed electrical model. Firstly, the chi-square parameter was used by Pearson [32]. However, in the case of static measurements, $\chi^{2.}$ cannot be regarded as an absolute, unequivocal measure of the data fitting, because it is not possible to determine whether a global or local minimum was reached. Moreover, the value of the correlation parameter χ^2 also depend on the quality of experimental measurements. In many cases, in particular in the case of potentiostatic measurements, it is difficult to keep a stationarity condition of the investigated object. The situation is different for dynamic measurements, where it is possible to describe the course of this quantity versus the current. The quality of the fitting of the proposed equivalent circuit is shown in Fig. 3g, as a dependence between χ^2 statistics and the fuel cell load. The values of χ^2 are within a single order of magnitude (10^{-5}) over the entire current range. There is no clear extremum of χ^2 for any current density value and no deterministic trend of the curve can be observed. The mean value of χ^2 equals (6.11 ± 1.30) x10^{-5} . This is a confirmation of the proper selection of the equivalent circuit from a statistical standpoint in the entire current range.

Fig.3g.

3.4. Coherence between the impedance spectra and the DC measurements

In case of the classic impedance measurements, where the utilized frequencies do not provide a full impedance spectrum, which one terminating at the imaginary impedance value approaching zero, we

are not able to determine the accuracy of the performed impedance analysis of obtained spectrum. This is due to the restricted frequency band of the traditional EIS measurement, the low-frequency limit of the spectrum is estimated with a degree of uncertainty. During DEIS measurements, the current and potential courses are analysed by means of their Fourier transforms including at a frequency of 0 Hz, which corresponds to the DC measurement [18], [19]. The simultaneous application of DC measurements and the DEIS method offers the possibility to find instantaneous values of the impedance in the entire current range, which allows verification of the finite character of the spectra and verification of the coherence between the AC and DC measurements. Apart from the frequencies contained in the multi-sinusoidal perturbation signal, one obtains an additional frequency equal to 0 Hz, determined from the DC measurements via calculation of the polarization resistance $R_p(i) = \left(\frac{dU(i)}{di}\right)_{i_p}$ from the current-voltage characteristics shown in Fig. 4a.

Fig. 4a.

$$\lim_{\omega \to 0} Z_{FC}(j\omega, i) = R_M(i) + R_{MCI}(i) + R_{CT}(i) + R_D(i) = R_p(i) \quad (7)$$

This dependence gives an opportunity, using a simple comparison, to determine the coherence between the AC and DC measurements as well as the complete character of the spectra and the precision of the performed analysis.

Fig. 4b shows a comparison of the sum of resistance and $R_p(i)$ values for an entire range of investigated load. As the analysis of the impedance spectra is always burdened with a certain error, the presented curve includes the error bars. It can be observed that the value of $R_p(i)$ practically overlaps the resistance sum over the entire investigated range. Despite limiting the measurement frequencies to 5Hz, the impedance spectra analysis provides the full characteristics of the tested object. The coherence between the DC and impedance results is further evidence for the selected equivalent circuit.

Fig. 4b.

Summary and Conclusions

A combination of direct and alternating current measurements not only provide verification of the completeness and accuracy of the impedance results, but more importantly it allows one to obtain instantaneous impedance spectra against the function of current. This provided a description of the influence of processes occurring in the fuel cell on its operation and upon varying current load. The presented dependencies of the equivalent circuit's parameters, against the current, gave a comprehensive impedance characteristic of the proton exchange membrane fuel cell operation. The current range is optimal when the charge transfer and diffusion resistance values reach a minimum.

This is owed to the fact that these electrochemical processes occur with the least impediments. For the same range of current, the local maximum of the capacitance values is also observed. Moreover, the authors present a possibility for the evaluation of the diffusion layer thickness changes depending on the magnitude of generated energy. It is not possible to quickly determine the optimal current conditions using classic impedance measurements. The Dynamic Electrochemical Impedance Spectroscopy methodology presented in this paper allows us to obtain reliable results under dynamic working conditions. This allows the use of this method as an online tool for monitoring and diagnostics of the fuel cell during operation. Dynamic impedance measurement can also be successfully used as a helpful tool in the process of designing fuel cells.

Acknowledgments

The research leading to the presented results has received funding from The National Centre for Research and Development (NCBR, Poland) under the Grant No. STAIR/6/2016 and the Federal Ministry of Education and Research (BMBF, Germany), the Grant No.: 01LX1601. The work was realized in the COALA project (control algorithm and controller for increasing the efficiency of hybrid PEMFC systems in different applications) in the framework of the Polish-German Sustainability Research Call (STAIR II).

[1] Mai T, Cole W, Reimers A. Setting cost targets for zero-emission electricity generation technologies. Applied Energy 2019;250:582–92. doi:10.1016/j.apenergy.2019.05.001.
[2] Conte M. ENERGY | Hydrogen Economy. Encyclopedia of Electrochemical Power Sources, Elsevier; 2009, p. 232–54. doi:10.1016/B978-044452745-5.00084-8.
[3] Zhang T, Wang P, Chen H, Pei P. A review of automotive proton exchange membrane fuel cell degradation under start-stop operating condition. Applied Energy 2018;223:249–62. doi:10.1016/j.apenergy.2018.04.049.
[4] Löbberding L, Madlener R. Techno-economic analysis of micro fuel cell cogeneration and storage in Germany. Applied Energy 2019;235:1603–13. doi:10.1016/j.apenergy.2018.11.023.
[5] Sulaiman N, Hannan MA, Mohamed A, Ker PJ, Majlan EH, Wan Daud WR. Optimization of energy management system for fuel-cell hybrid electric vehicles: Issues and recommendations. Applied Energy 2018;228:2061–79. doi:10.1016/j.apenergy.2018.07.087.
[6] Antolini E, Giorgi L, Pozio A, Passalacqua E. Influence of Nafion loading in the catalyst layer of gas-diffusion electrodes for PEFC. Journal of Power Sources 1999;77:136–42. doi:10.1016/S0378-7753(98)00186-4.
[7] Shi Z, Wang X, Draper O. Effect of Porosity Distribution of Gas Diffusion Layer on Performance of Proton Exchange Membrane Fuel Cells. vol. 11, ECS; 2007, p. 637–46. doi:10.1149/1.2780977.
[8] Kumbur EC, Mench MM. FUEL CELLS – PROTON-EXCHANGE MEMBRANE FUEL CELLS | Water Management. Encyclopedia of Electrochemical Power Sources, Elsevier; 2009, p. 828–47. doi:10.1016/B978-044452745-5.00862-5.
[9] Niu Z, Bao Z, Wu J, Wang Y, Jiao K. Two-phase flow in the mixed-wettability gas diffusion layer of proton exchange membrane fuel cells. Applied Energy 2018;232:443–50. doi:10.1016/j.apenergy.2018.09.209.

[10] Li Y, Yang J, Song J. Structure models and nano energy system design for proton exchange membrane fuel cells in electric energy vehicles. Renewable and Sustainable Energy Reviews 2017;67:160–72. doi:10.1016/j.rser.2016.09.030.
[11] El-kharouf A, Mason TJ, Brett DJL, Pollet BG. Ex-situ characterisation of gas diffusion layers for proton exchange membrane fuel cells. Journal of Power Sources 2012;218:393–404. doi:10.1016/j.jpowsour.2012.06.099.
[12] Slepski P, Janicka E, Darowicki K, Pierozynski B. Impedance monitoring of fuel cell stacks. Journal of Solid State Electrochemistry 2015;19:929–33. doi:10.1007/s10008-014-2676-8.
[13] Darowicki K, Janicka E, Slepski P. Study of Direct Methanol Fuel Cell Process Dynamics Using Dynamic Electrochemical Impedance Spectroscopy. INTERNATIONAL JOURNAL OF ELECTROCHEMICAL SCIENCE 2012;7:12090–7.
[14] Darowicki K, Gawel L. Impedance Measurement and Selection of Electrochemical Equivalent Circuit of a Working PEM Fuel Cell Cathode. Electrocatalysis 2017;8:235–44. doi:10.1007/s12678-017-0363-0.
[15] Slepski P, Darowicki K, Janicka E, Lentka G. A complete impedance analysis of electrochemical cells used as energy sources. Journal of Solid State Electrochemistry 2012;16:3539–49. doi:10.1007/s10008-012-1825-1.
[16] Wysocka J, Krakowiak S, Ryl J, Darowicki K. Investigation of the electrochemical behaviour of AA1050 aluminium alloy in aqueous alkaline solutions using Dynamic Electrochemical Impedance Spectroscopy. Journal of Electroanalytical Chemistry 2016;778:126–36. doi:10.1016/j.jelechem.2016.08.028.
[17] Darowicki K, Ślepski P, Szociński M. Application of the dynamic EIS to investigation of transport within organic coatings. Progress in Organic Coatings 2005;52:306–10. doi:10.1016/j.porgcoat.2004.06.007.
[18] Darowicki K. Theoretical description of the measuring method of instantaneous impedance spectra. Journal of Electroanalytical Chemistry 2000;486:101–5. doi:10.1016/S0022-0728(00)00110-8.
[19] Darowicki K, Orlikowski J, Lentka G. Instantaneous impedance spectra of a non-stationary model electrical system. Journal of Electroanalytical Chemistry 2000;486:106–10. doi:10.1016/S0022-0728(00)00111-X.
[20] Cahan BD. AC Impedance Investigations of Proton Conduction in Nafion™. Journal of The Electrochemical Society 1993;140:L185. doi:10.1149/1.2221160.
[21] Wintersgill MC, Fontanella JJ. Complex impedance measurements on Nafion. Electrochimica Acta 1998;43:1533–8. doi:10.1016/S0013-4686(97)10049-4.
[22] Makharia R, Mathias MF, Baker DR. Measurement of Catalyst Layer Electrolyte Resistance in PEFCs Using Electrochemical Impedance Spectroscopy. Journal of The Electrochemical Society 2005;152:A970. doi:10.1149/1.1888367.
[23] Reshetenko T, Kulikovsky A. Impedance Spectroscopy Study of the PEM Fuel Cell Cathode with Nonuniform Nafion Loading. Journal of The Electrochemical Society 2017;164:E3016–21. doi:10.1149/2.0041711jes.
[24] Song C, Tang Y, Zhang JL, Zhang J, Wang H, Shen J, et al. PEM fuel cell reaction kinetics in the temperature range of 23–120°C. Electrochimica Acta 2007;52:2552–61. doi:10.1016/j.electacta.2006.09.008.
[25] Singh RK, Devivaraprasad R, Kar T, Chakraborty A, Neergat M. Electrochemical Impedance Spectroscopy of Oxygen Reduction Reaction (ORR) in a Rotating Disk Electrode Configuration: Effect of Ionomer Content and Carbon-Support. Journal of the Electrochemical Society 2015;162:F489–98. doi:10.1149/2.0141506jes.
[26] Paulus UA, Schmidt TJ, Gasteiger HA, Behm RJ. Oxygen reduction on a high-surface area Pt/Vulcan carbon catalyst: a thin-film rotating ring-disk electrode study. Journal of Electroanalytical Chemistry 2001;495:134–45. doi:10.1016/S0022-0728(00)00407-1.

[27] Wagner N, Friedrich KA. FUEL CELLS – PROTON-EXCHANGE MEMBRANE FUEL CELLS | Dynamic Operational Conditions. Encyclopedia of Electrochemical Power Sources, Elsevier; 2009, p. 912–30. doi:10.1016/B978-044452745-5.00239-2.
[28] Darowicki K, Janicka E, Mielniczek M, Zielinski A, Gawel L, Mitzel J, et al. Implementation of DEIS for reliable fault monitoring and detection in PEMFC single cells and stacks. Electrochimica Acta 2018. doi:10.1016/j.electacta.2018.09.105.
[29] Kulikovsky AA, Eikerling M. Analytical solutions for impedance of the cathode catalyst layer in PEM fuel cell: Layer parameters from impedance spectrum without fitting. Journal of Electroanalytical Chemistry 2013;691:13–7. doi:10.1016/j.jelechem.2012.12.002.
[30] Paik CH, Jarvi TD, O'Grady WE. Extent of PEMFC Cathode Surface Oxidation by Oxygen and Water Measured by CV. Electrochemical and Solid-State Letters 2004;7:A82. doi:10.1149/1.1649698.
[31] Boukamp B. A Nonlinear Least Squares Fit procedure for analysis of immittance data of electrochemical systems. Solid State Ionics 1986;20:31–44. doi:10.1016/0167-2738(86)90031-7.
[32] Pearson K. X. *On the criterion that a given system of deviations from the probable in the case of a correlated system of variables is such that it can be reasonably supposed to have arisen from random sampling*. The London, Edinburgh, and Dublin Philosophical Magazine and Journal of Science 1900;50:157–75. doi:10.1080/14786440009463897.

Figure

Click here to download high resolution image

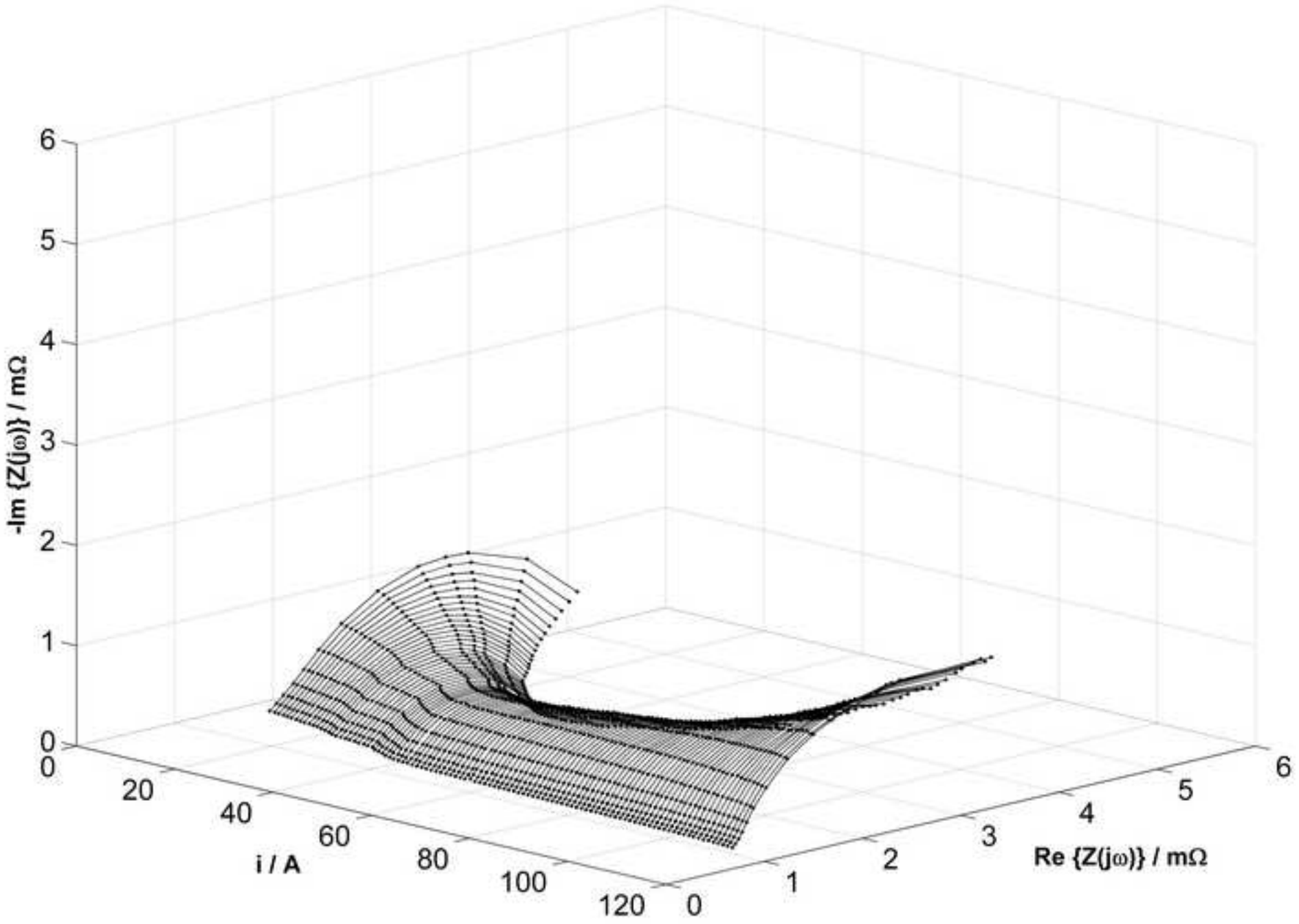

Figure

Click here to download high resolution image

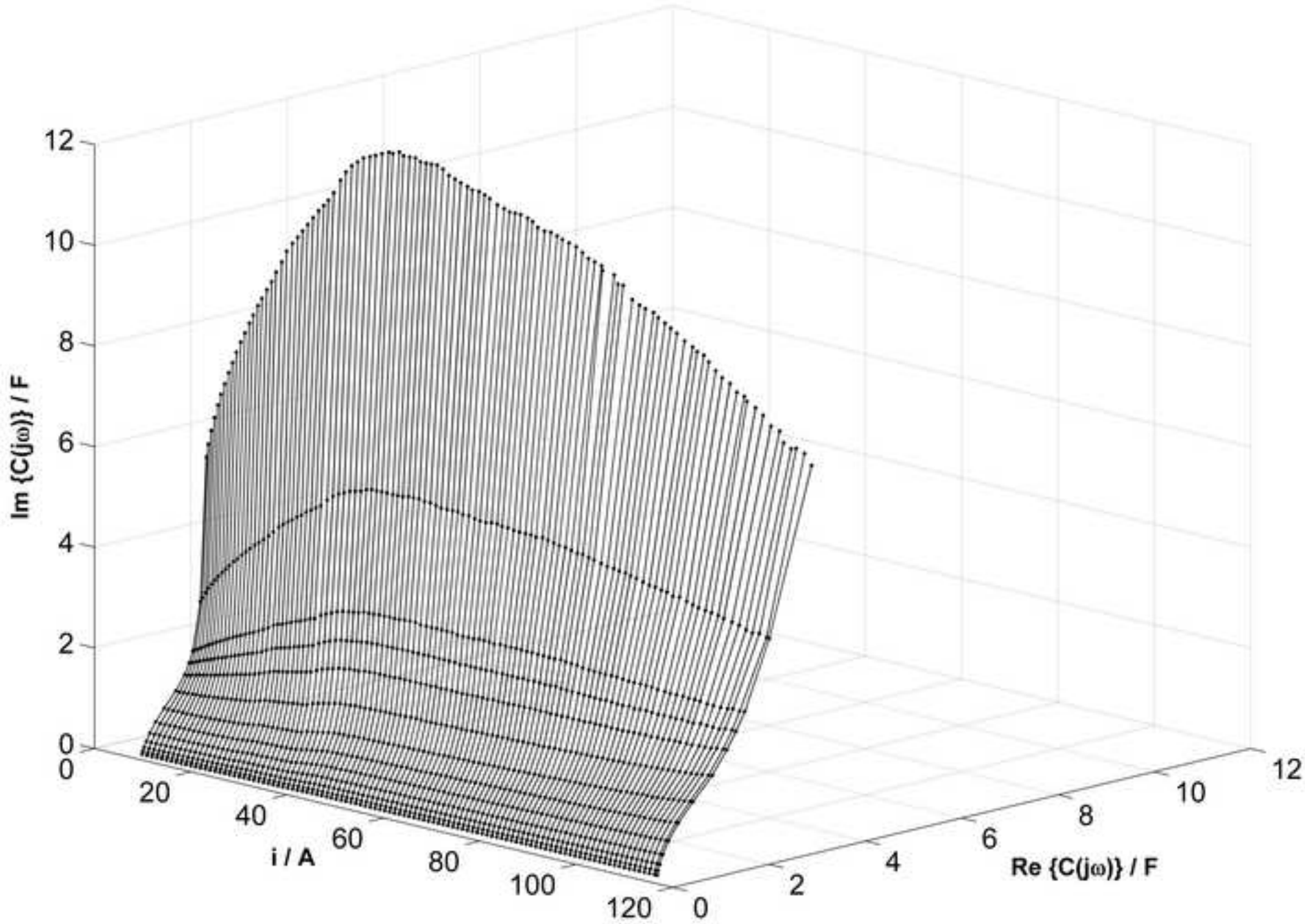

Figure

Click here to download high resolution image

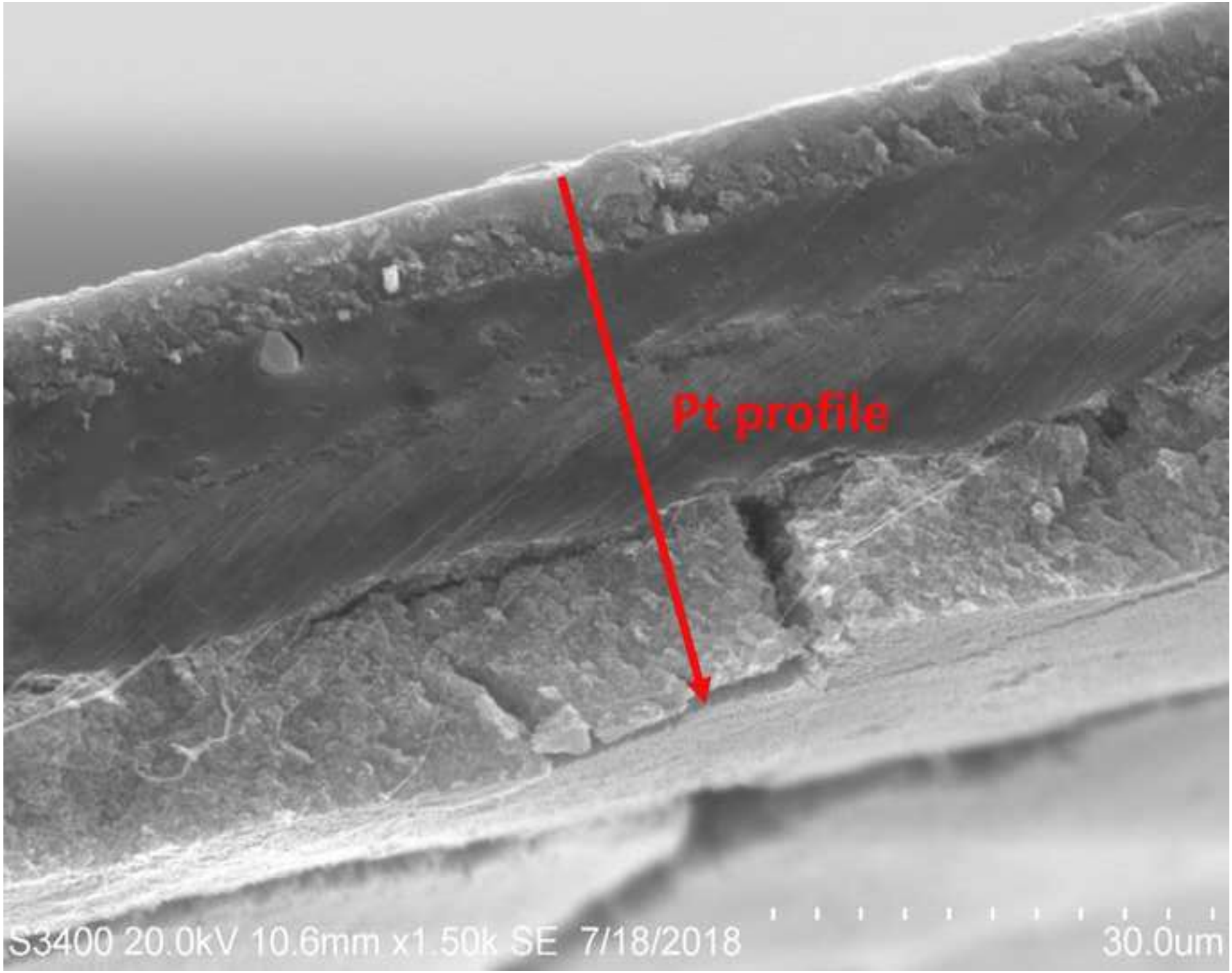

Figure

Click here to download high resolution image

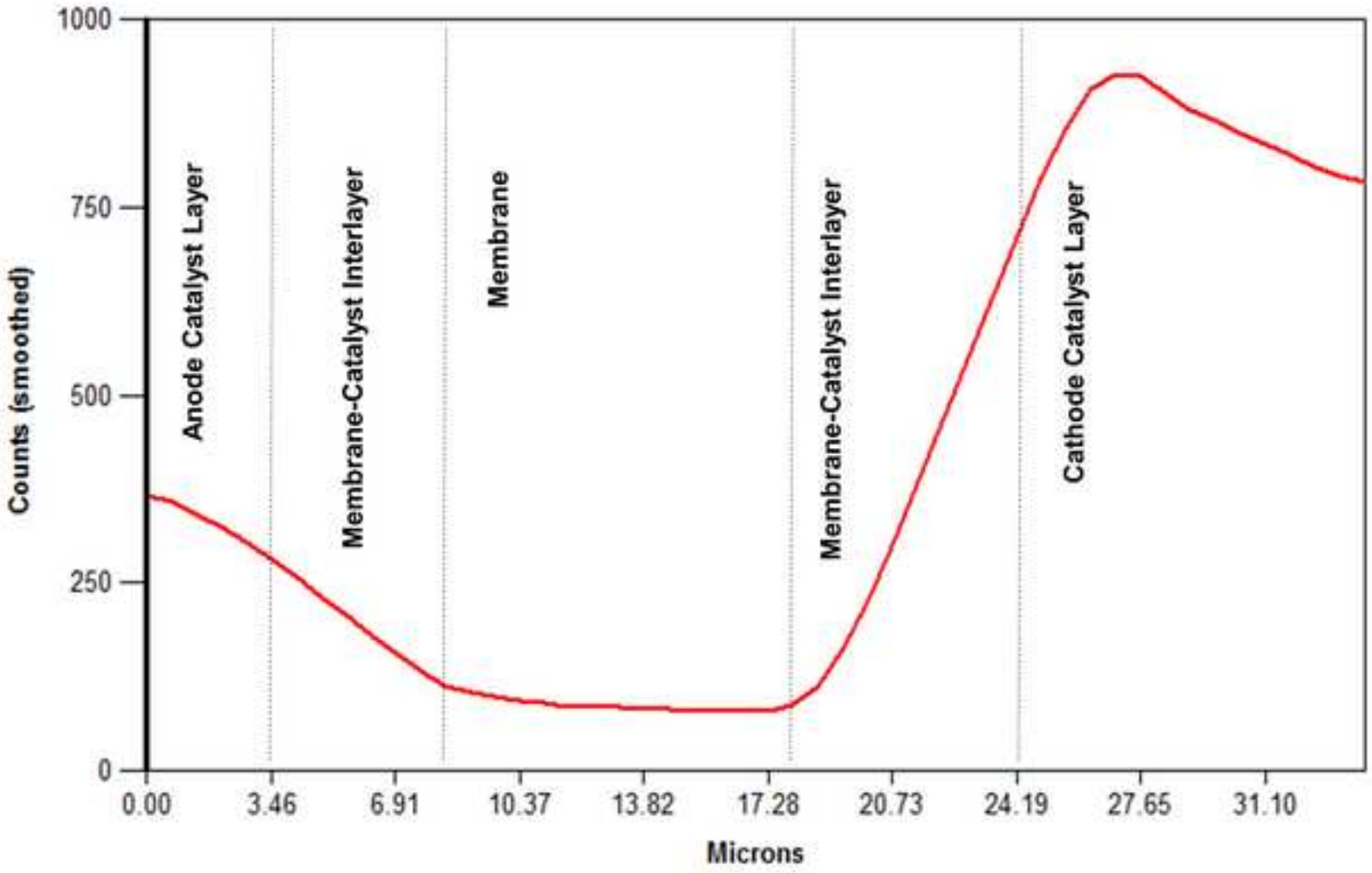

Figure
Click here to download high resolution image

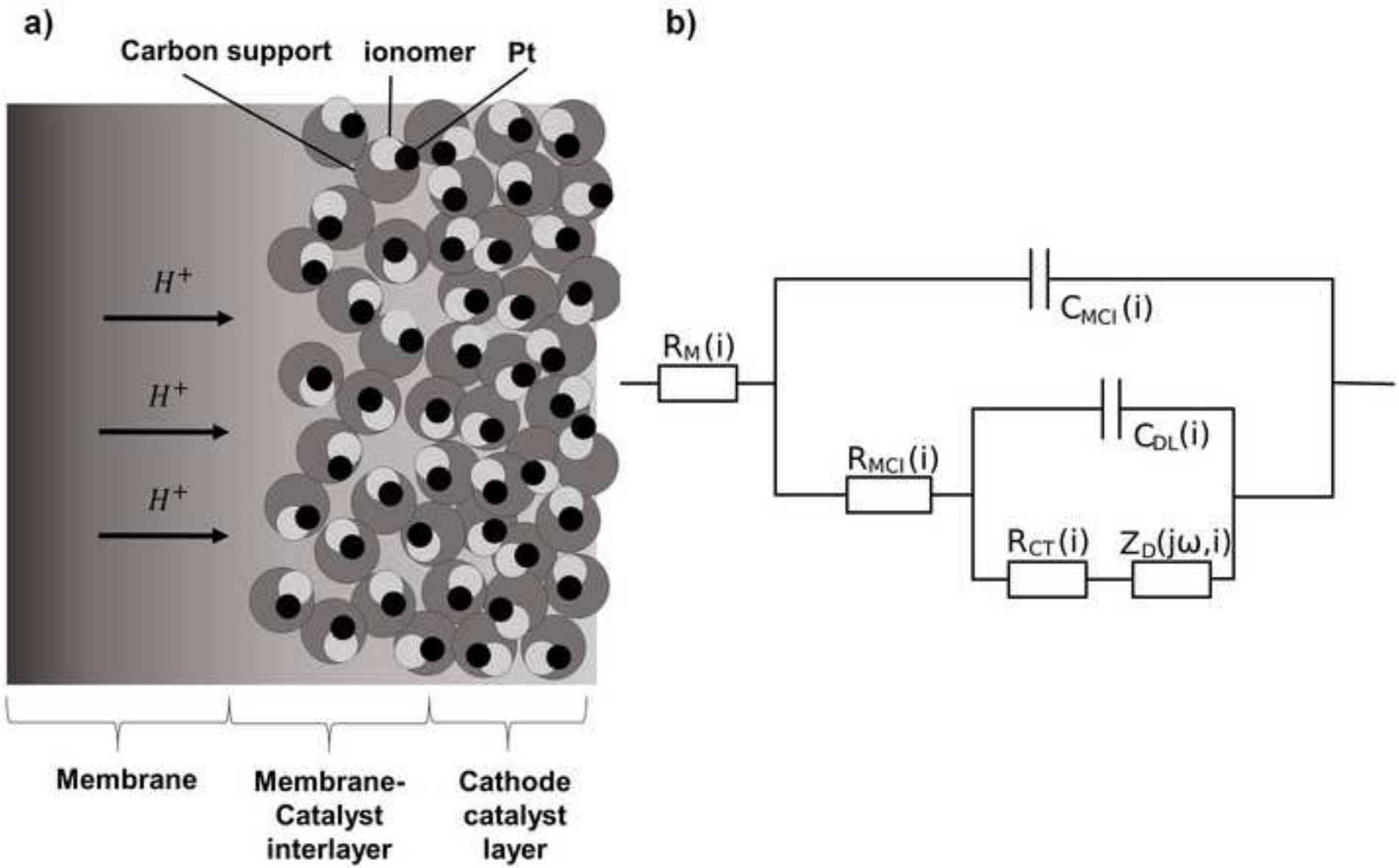

Figure

Click here to download high resolution image

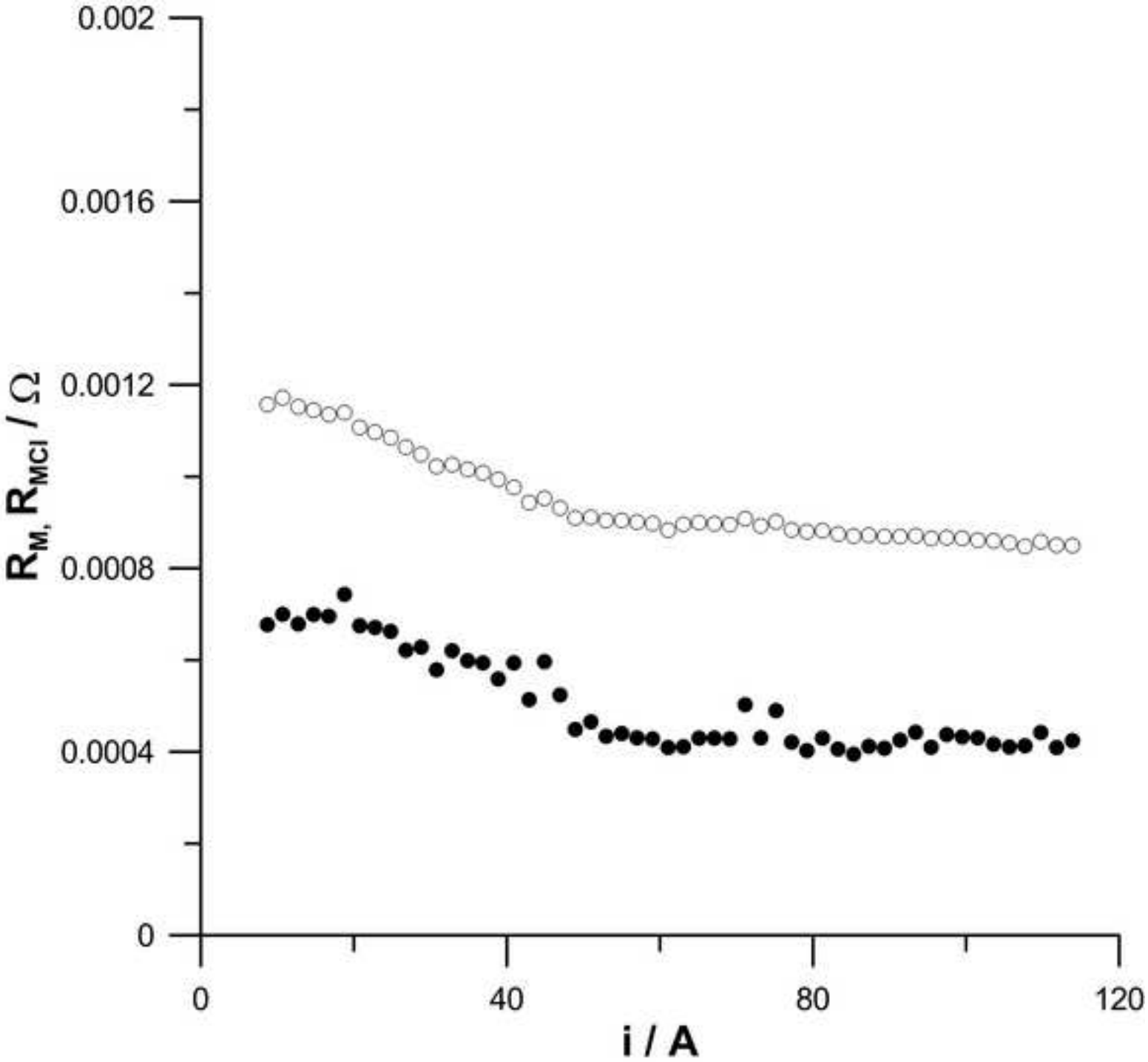

Figure

Click here to download high resolution image

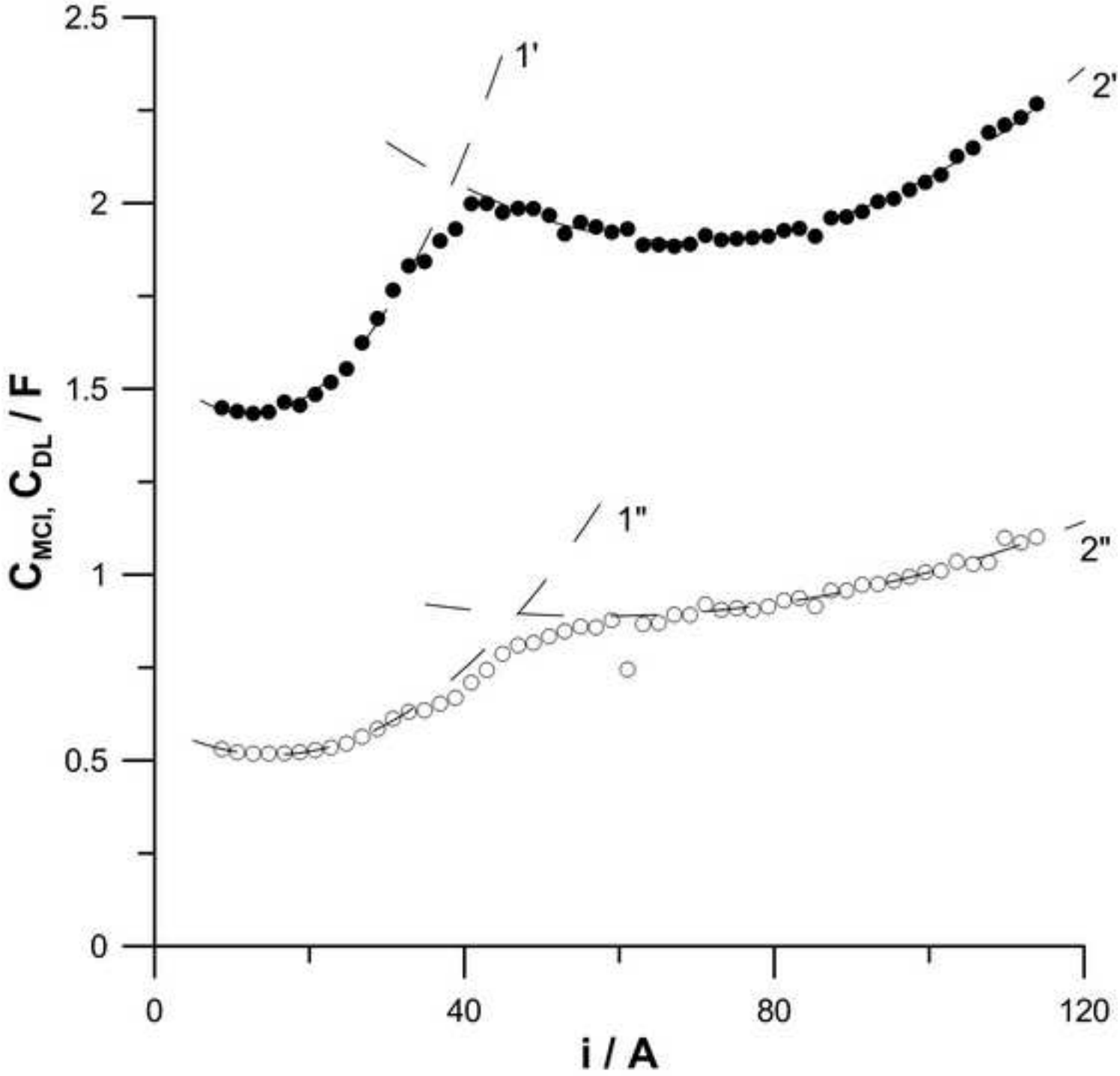

Figure

Click here to download high resolution image

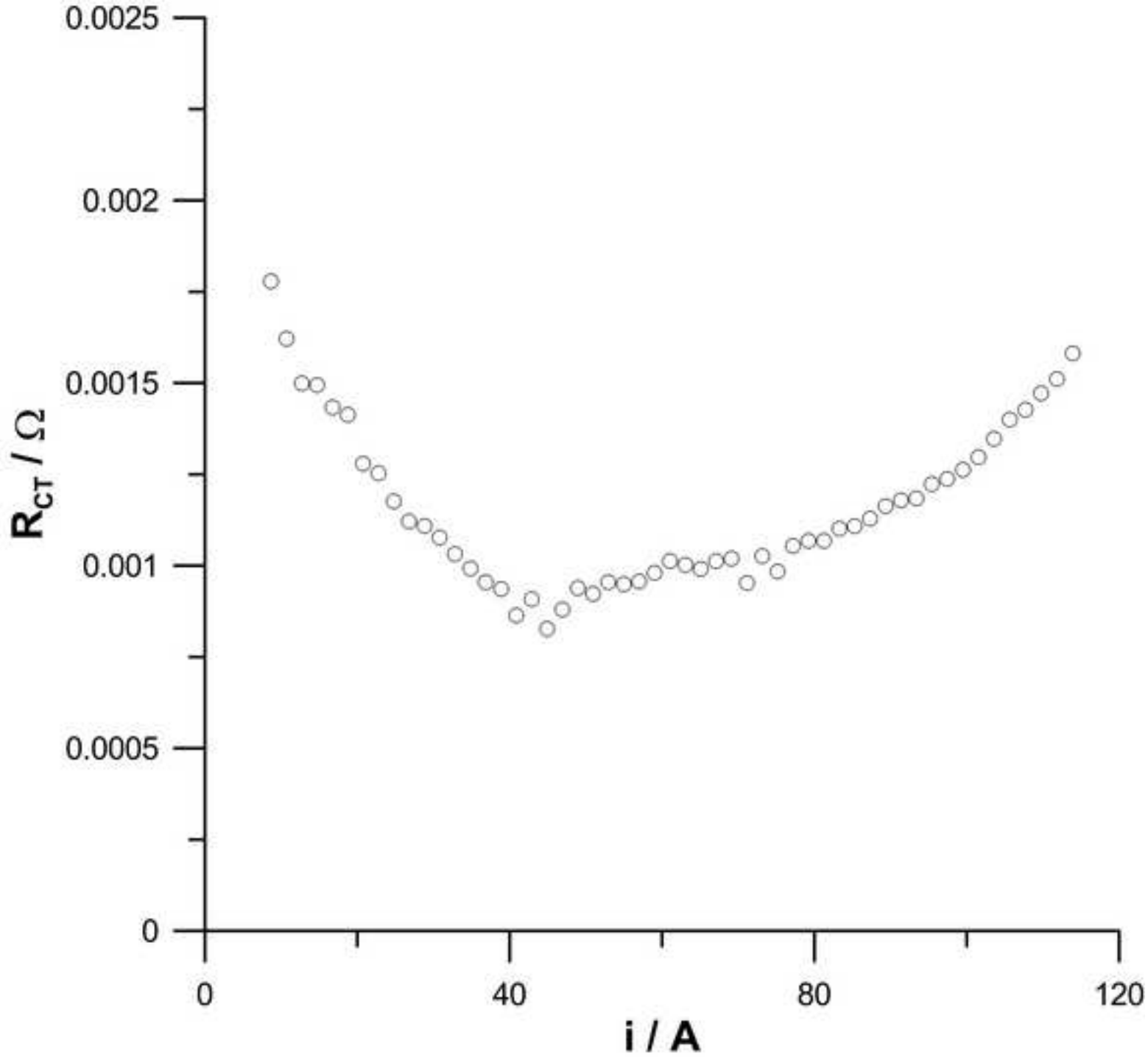

Figure

Click here to download high resolution image

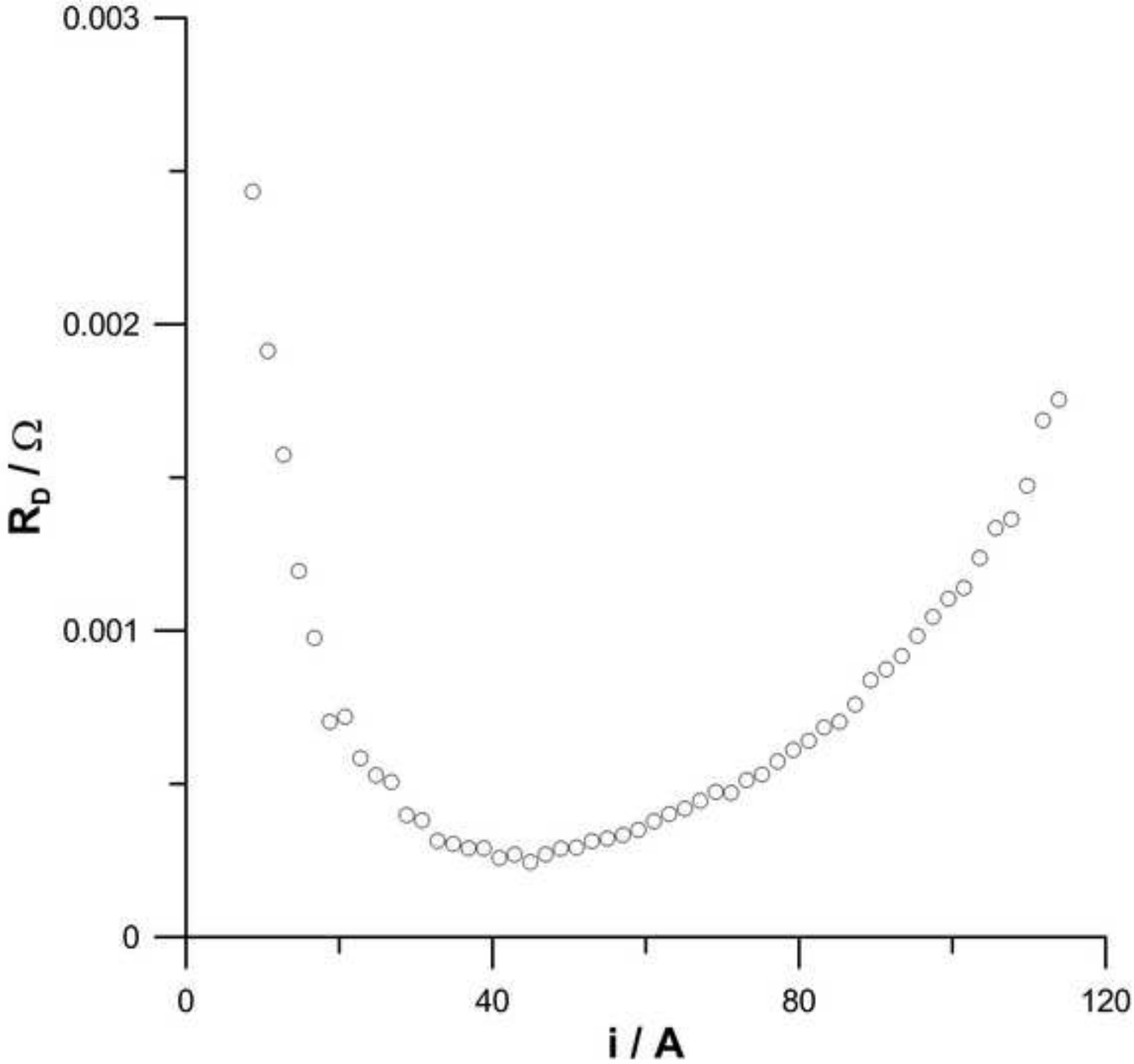

Figure

Click here to download high resolution image

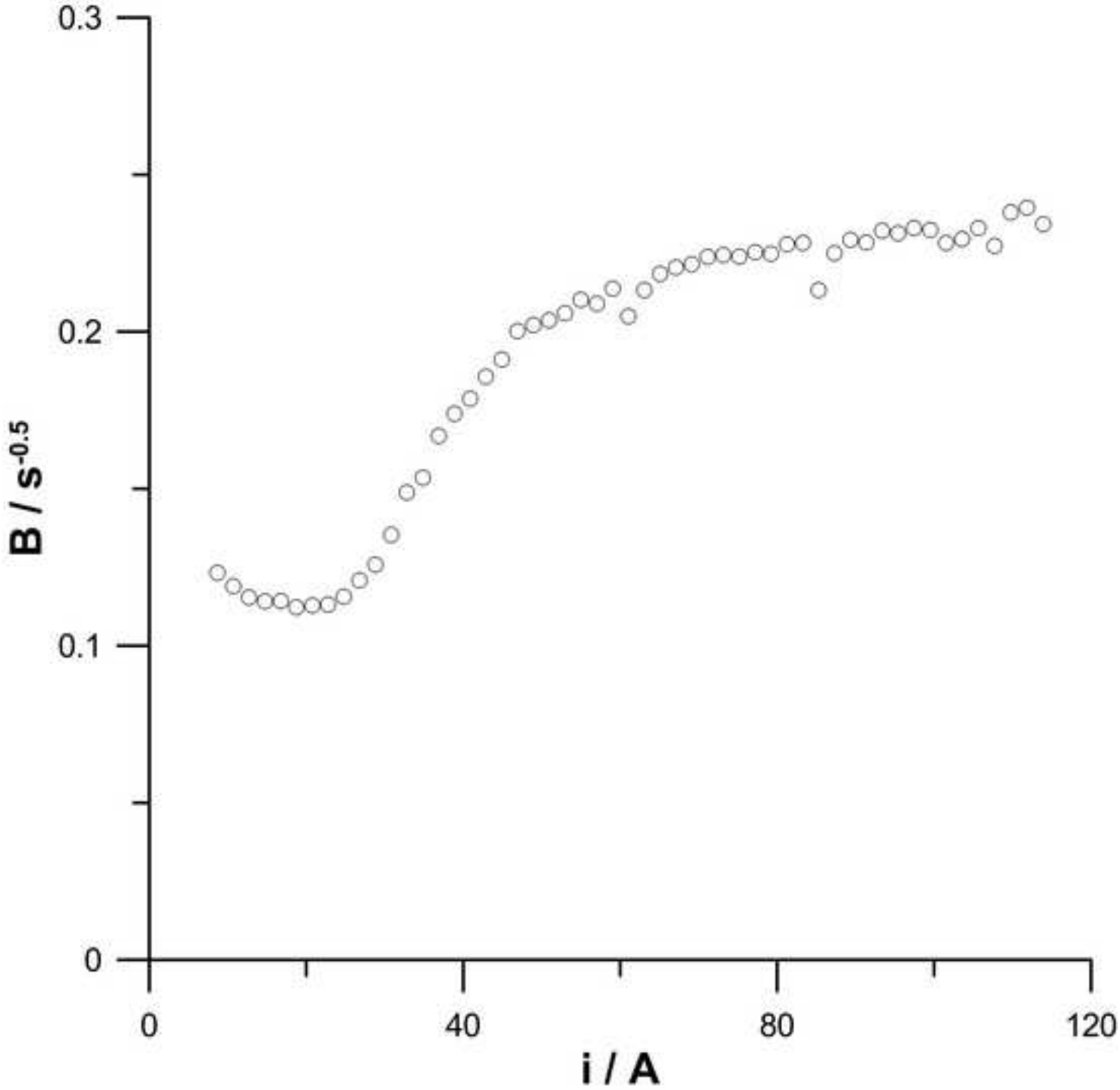

Figure

Click here to download high resolution image

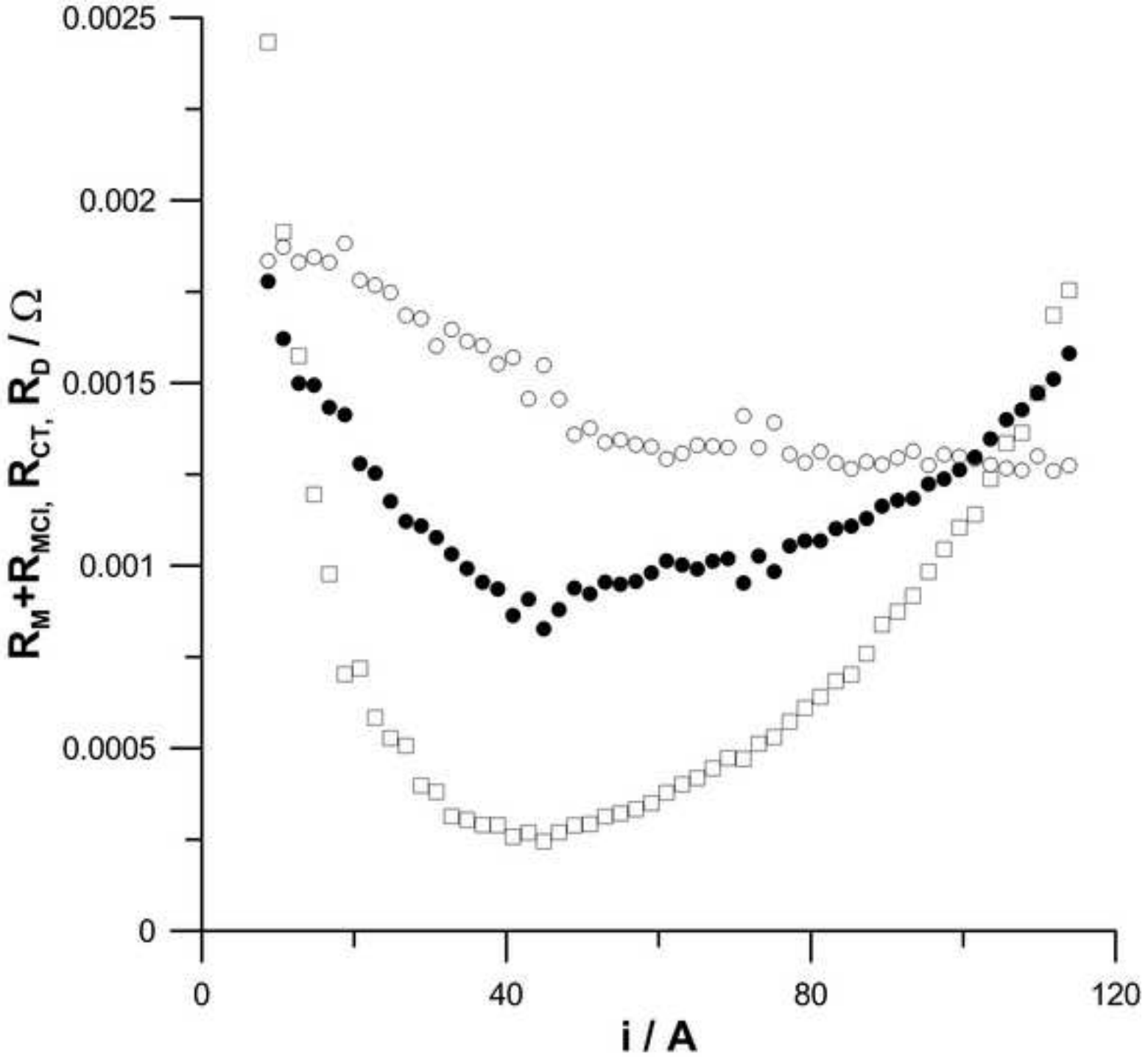

Figure
Click here to download high resolution image

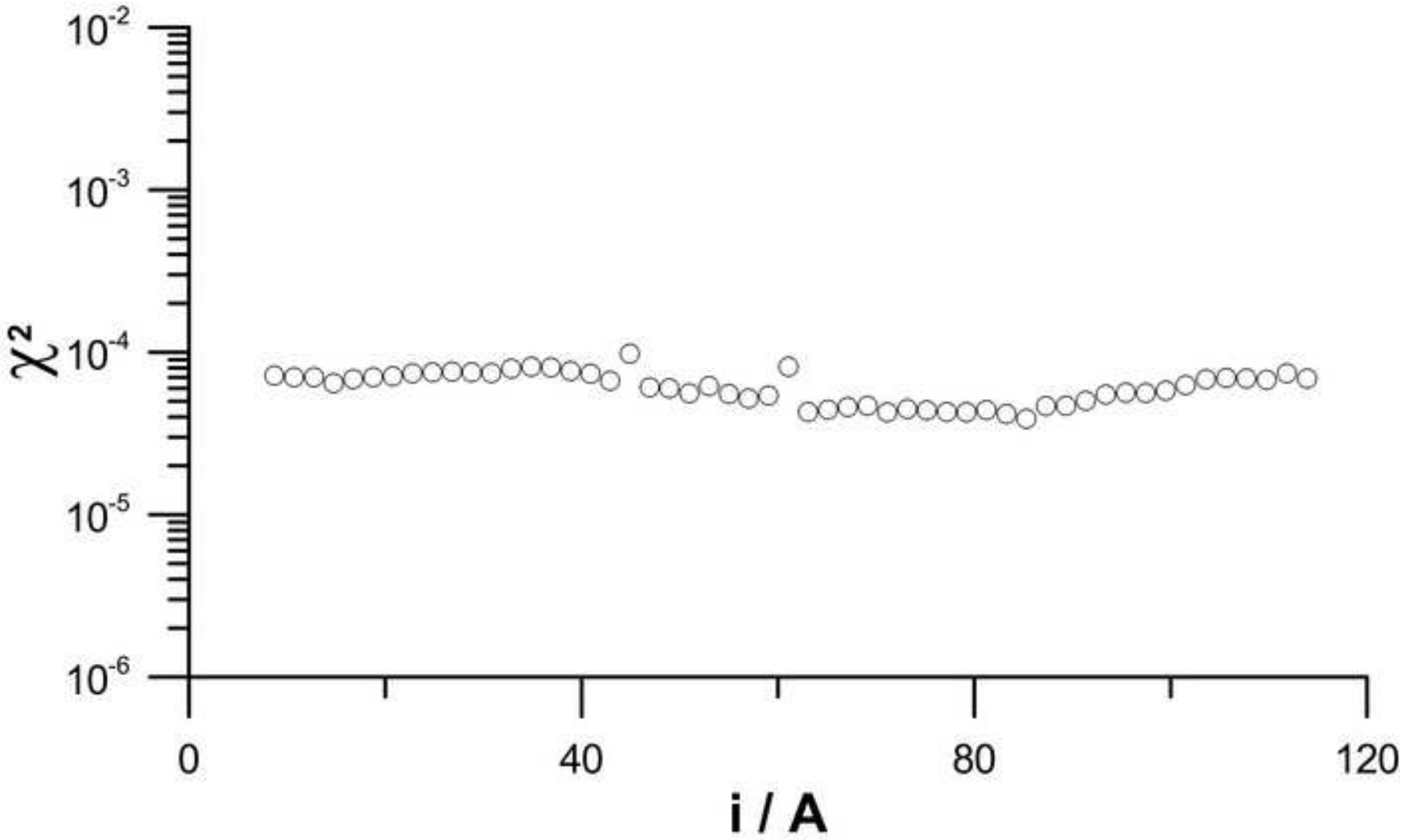

Figure

Click here to download high resolution image

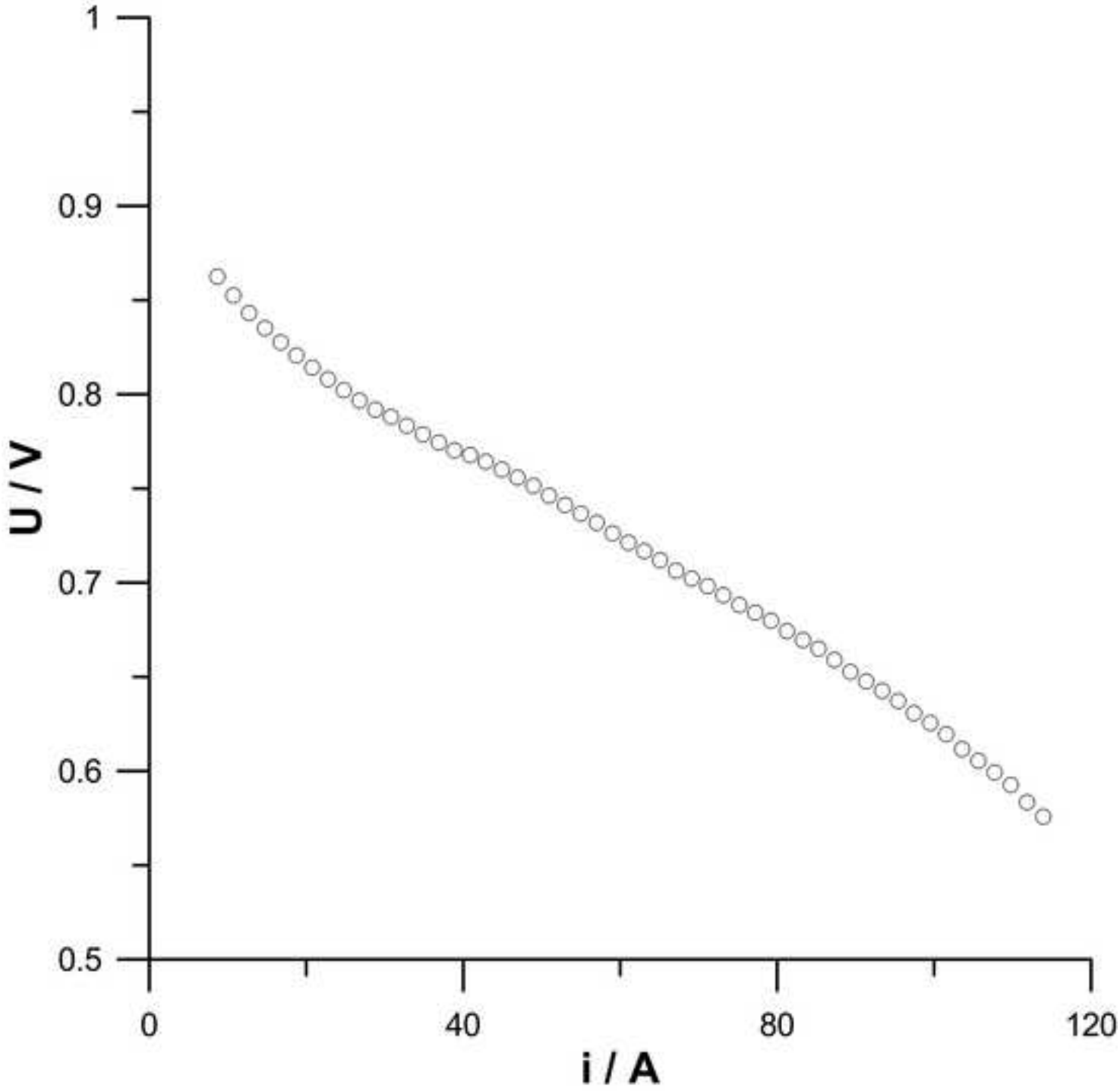

Figure

Click here to download high resolution image

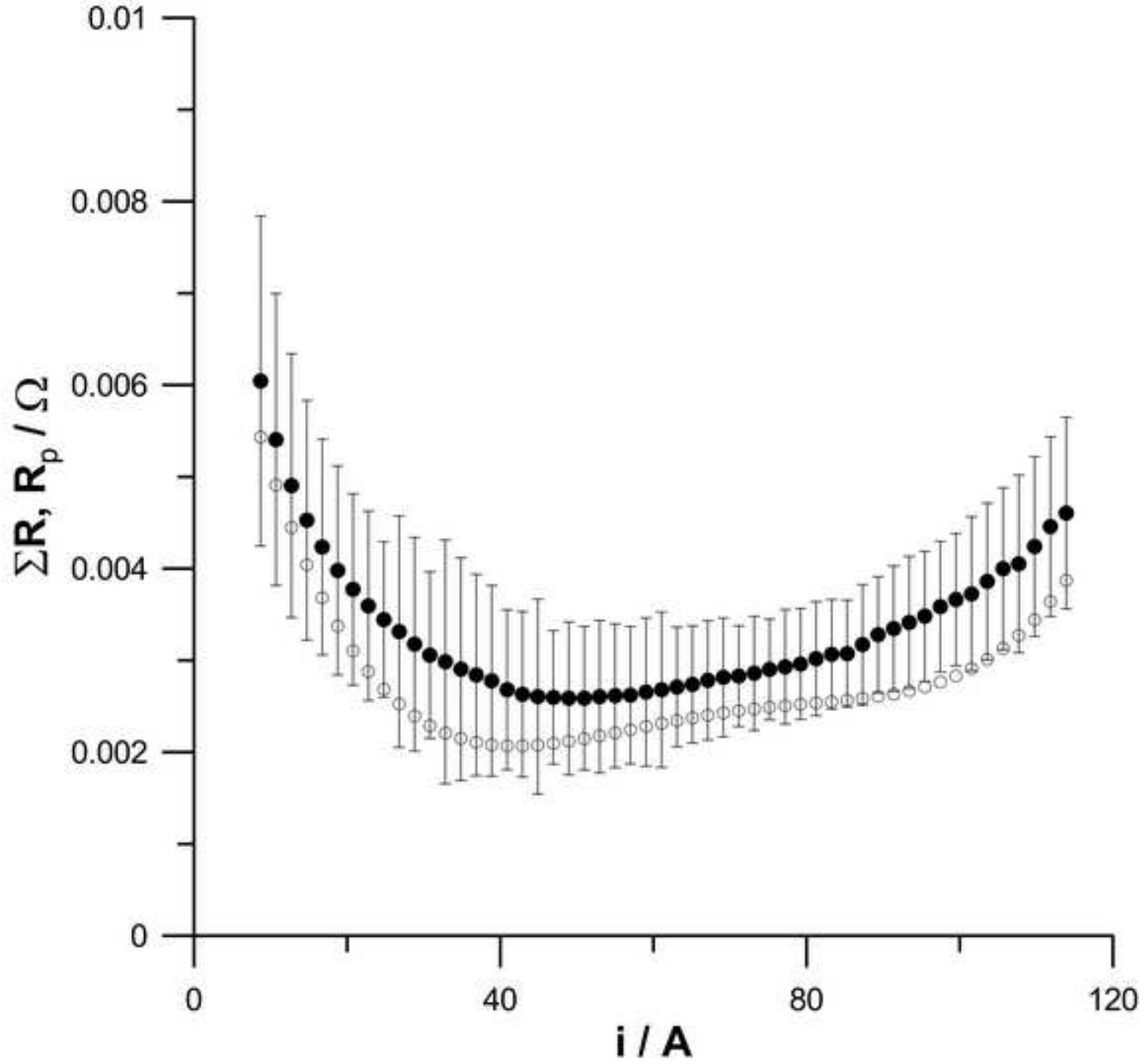

Figure Captions

Fig. 1a. Impedance diagram for PEM fuel cell obtained in galvanodynamic mode. Geometric surface S=96 cm^2, current load change rate di/dt = 50 mA s^{-1}, measurement frequencies range from 5Hz to 1123 Hz.

Fig. 1b. Complex capacitance diagram for PEM fuel cell obtained in galvanodynamic mode. Geometric surface S=96 cm^2, current load change rate di/dt = 50 mA s^{-1}, measurement frequencies range from 5Hz to 1123 Hz.

Fig.2a. SEM image of MEA cross section (magnification x1500)

Fig.2b. Platinum content profile, based on the number of counts, along the entire MEA thickness, obtained with energy-dispersive X-ray spectroscopy (EDX), using UltraDry Detector by the Thermo Fisher Scientific

Fig. 2. c) Scheme of MEA cathodic part cross-section, d) Electrical equivalent circuit employed for analysis of instantaneous impedance spectra. $R_M(i)$ – instantaneous resistance of the membrane, $R_{MCI}(i)$ – instantaneous resistance of the interlayer, $R_{CT}(i)$ – instantaneous charge transfer resistance, $Z_D(j\omega, i)$ – instantaneous impedance of the element describing diffusion in a finite thickness layer, $C_{MCI}(i)$ – instantaneous capacitance of the catalyst layer, $C_{DL}(i)$ – instantaneous capacitance of the electrical double layer.

Fig.3a. Instantaneous value of $R_{MCI}(i)$ (●) and $R_M(i)$ (○) versus current. Geometric surface S=96 cm^2, current load change rate di/dt = 50 mA s^{-1}

Fig.3b. Instantaneous value of$C_{DL}(i)$ (●) and $C_{MCI}(i)$ (○) versus current. Geometric surface S=96 cm^2, current load change rate di/dt = 50 mA s^{-1}

Fig.3c. Instantaneous value of charge transfer resistance versus current. Geometric surface S=96 cm^2, current load change rate di/dt = 50 mA s^{-1}

Fig.3d. Instantaneous value of diffusion resistance versus current. Geometric surface S=96 cm^2, current load change rate di/dt = 50 mA s^{-1}

Fig.3e. Parameter $B(i)$ versus current. Geometric surface S=96 cm^2, current load change rate di/dt = 50 mA s^{-1}

Fig. 3f. Instantaneous resistances $R_M(i) + R_{MCI}(i)$ (○), $R_{CT}(i)$ (●) , $R_D(i)$ (□) versus current. Geometric surface S=96 cm^2, current load change rate di/dt = 50 mA s^{-1}

Fig.3g. Distribution of χ^2 parameter versus current density.

Fig. 4a. Current-voltage characteristics obtained simultaneously with impedance characteristics. Geometric surface S=96 cm^2, current load change rate di/dt = 50 mA s^{-1}

Fig. 4b. Comparison of $R_p(i)$ value (○) and sum of resistances obtained from impedance analysis (●)